Publication P4

Kristjan Tabri, Jerzy Matusiak, and Petri Varsta. 2009. Sloshing interaction in ship collisions—An experimental and numerical study. Ocean Engineering, volume 36, numbers 17-18, pages 1366-1376.

Ocean Engineering 36 (2009) 1366–1376

Contents lists available at ScienceDirect

Ocean Engineering

journal homepage: www.elsevier.com/locate/oceaneng

Sloshing interaction in ship collisions—An experimental and numerical study

Kristjan Tabri *, Jerzy Matusiak, Petri Varsta

Helsinki University of Technology, Department of Applied Mechanics, Marine Technology, P.O. Box 5300, 02015 TKK, Finland

ARTICLE INFO

Article history:
Received 25 March 2009
Accepted 30 August 2009
Available online 10 September 2009

Keywords:
Collision dynamics
Sloshing interaction
Model-scale experiments

ABSTRACT

Sloshing interaction in ship collisions is studied both experimentally and numerically. The rapid change in ship motions resulting from contact loading in collisions initiates violent sloshing inside partially filled liquid tanks on board. Sloshing affects the collision dynamics and reduces the amount of energy available for structural deformations. An understanding of this interaction phenomenon was obtained by a series of model-scale experiments, in which a striking ship, with two partially filled tanks, collided with an initially motionless struck ship without any liquid on board. The influence on the structural deformation of the fluid mass in the tanks and the velocity of the collision was studied. Numerical simulations of the cases were performed, combining a linear sloshing model with a theoretical collision model. The simulation model was validated with experimental results and good agreement was achieved in the case of medium filling levels in the tanks, while correspondingly the deformation energy was overestimated by up to 10% for shallow filling levels.

1. Introduction

Large-scale ship collision experiments (Wevers and Vredeveldt, 1999) revealed that fluid sloshing in partially filled tanks had a significant effect on the dynamics of ship collisions (Tabri et al., 2009a, b). These large-scale experiments between two river tankers aimed to study the performance of different structural concepts and to gain insight into the collision dynamics. To obtain the desired ship drafts, some tanks of the ships were only partially filled, making it possible for water sloshing to occur. Here, we exploit the outcomes of two large-scale experiments—Y-core test with a large number of partially filled tanks on board of both ships (Wevers and Vredeveldt, 1999) and X-core tests with only insignificant amount of water in partially filled tanks (Wolf, 2003). It is known that under external dynamic excitation partially filled tanks with fluids are prone to violent sloshing, in which the eigenperiods of the fluid oscillations depend on the depth of the fluid and on the horizontal dimensions of the tank. The effect of sloshing on collision dynamics is through time varying loads exerted on the containing ship structures and by storing part of the kinetic energy. In a collision, the sloshing is initiated by a rapid change in the motion of the ship. If the amount of sloshing fluid is significant compared to the total mass of the ship, the distribution of energy components in the collision is changed. Conventional calculation methods used to simulate ship collisions do not normally include the sloshing interaction.

Numerical simulations of large-scale collision experiments (Tabri et al., 2009a, b) included the sloshing interaction for the first time, exploiting a mathematical model developed by Graham and Rodriguez (1952). This method is based on a linear potential flow theory. The correspondence between the results of the numerical simulations and those of the experiments was found to be good, proving the suitability of the sloshing model for collision simulations. In that large-scale experiment the ratio of the depth of the water to the dimensions of the tank in the sloshing direction was above 0.2, which is considered a lower bound for the applicability of the linear sloshing theory (Chen et al., 2008). The calculations revealed that the sloshing "stored" part of the kinetic energy and thus reduced the amount of energy available for structural deformations (Tabri et al., 2009a, b). The sloshing was more significant in the striking ship compared to the struck ship due to larger kinetic energy involved. Zhang and Suzuki (2007) studied the sloshing interaction during a collision numerically using the Lagrangian and arbitrary Lagrangian–Eulerian methods. On that basis, they concluded that the linear sloshing model underestimates the energy available for structural deformations by about 17% compared to more advanced numerical models, which include non-linear effects. However, in their simulations the tank was filled to up to 95% of its height and, therefore, the influence of roof impacts might be significant, presenting a rather unfavorable setup for the linear model.

In the large-scale experiments the sloshing took place in a number of partially filled tanks on board both ships and, thus, the concurrent interaction of several sloshing processes made it cumbersome to evaluate the pure sloshing phenomenon. To gain a deeper insight into this important phenomenon of sloshing, it was

* Corresponding author. Tel.: +358 94513392; fax: +358 94514173.
E-mail addresses: kristjan.tabri@tkk.fi, kristjan@mec.ee (K. Tabri).

0029-8018/$ - see front matter © 2009 Elsevier Ltd. All rights reserved.
doi:10.1016/j.oceaneng.2009.08.017

decided to carry out unique model-scale collision experiments, in which the direct influence of sloshing could be evaluated by comparing the results of tests with and without water in tanks. Hereafter, these experiments are referred to as wet or dry tests. The focus was placed on symmetric collision tests, where the striking ship model collided at a right angle to the amidships of the struck ship model. This simplified the influence of ship motions on the sloshing. Two tanks were installed on board the striking ship model, while the struck model did not carry any liquids on board.

In the present study, the linear sloshing model of Graham and Rodriguez (1952) is implemented in the collision model presented by Tabri et al. (2009), where the contact force model was improved compared to that of Tabri et al. (2009a, b). The aim of the study is to validate the calculation model with different water-filling levels and collision velocities, thus providing a validated numerical calculation model applicable for the structural design of ships in the conceptual stage.

2. Modeling of sloshing during collision

In a collision, the momentum of the striking ship is transmitted through contact loading to the initially motionless struck ship. When these two ships collide, their masses remain constant and the change in momentum is caused by the change in velocity. In collision dynamics, the total energy is composed as a sum of the kinetic energy E_K, deformation energy E_D, and of the work done to overcome the hydrodynamic forces. For symmetric collisions the deformation energy in respect to the initial kinetic energy of the striking ship, $E_K{}^A|_{t=0}$, can traditionally be estimated by Minorsky's (1959) formula:

$$\frac{E_D}{E_K^A|_{t=0}} = \frac{a_2^B + m^B}{(a_1^A + m^A) + (a_2^B + m^B)}, \tag{1}$$

where the superscript A refers to the striking ship and B to the struck ship. Term a_1 refers to the hydrodynamic added mass associated with the surge motion, a_2 is the sway added mass, and m is the mass of the ship. This model considers the inertia forces resulting from the total ship mass m and the hydrodynamic added mass a. Other components of the hydromechanical forces, such as frictional resistance, the restoring force, and the hydrodynamic damping, are excluded.

If one of the ships, or both, has partially filled liquid tanks with a free surface, the fluid inside the tank starts to slosh during the collision – see Fig. 1 – and interacts with the containing structure over a longer time span than would a rigidly fixed mass. Thus, the participation of the sloshing mass in the momentum transmission is delayed and Eq. (1) is not valid any more.

Time domain simulation models such as those of Petersen (1982), Brown (2002), Tabri et al. (2009a, b), etc. also consider only fixed masses and no fluids on board, but as they evaluate the whole time history of ship motions, the sloshing interaction can be included in these.

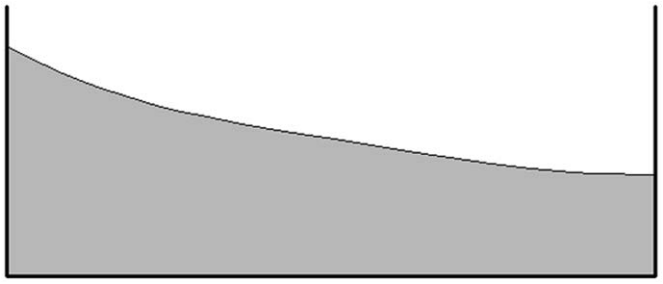

Fig. 1. Sloshing of liquid in partially filled tank.

2.1. Equations of motion of "dry" ship

In Tabri et al. (2009b) the equations of motion of a dry ship subjected to an external force **F** and moment **G** were presented in a form convenient for numerical simulations:

$$[\mathbf{M}_\mu]\begin{Bmatrix}\dot{\mathbf{u}}\\ \dot{\mathbf{\Omega}}\end{Bmatrix} + [\mathbf{M}_\mu^\Omega]\begin{Bmatrix}\mathbf{u}\\ \mathbf{\Omega}\end{Bmatrix} = \begin{Bmatrix}\mathbf{F}\\ \mathbf{G}\end{Bmatrix} - \mathbf{F}_\mu. \tag{2}$$

The scalar form of Eq. (2) considering all six degrees of freedom is presented in Appendix A. Besides the mass and inertia terms, the matrix $[\mathbf{M}_\mu]$ also contains the added mass coefficients describing the acceleration component of the radiation force $\mathbf{F}_\mu$, which makes it possible to subtract it from the total force **F** (Tabri et al., 2009b). Non-linear cross-coupling velocity terms, together with appropriate mass, inertia, and added mass coefficients, are given in $[\mathbf{M}_\mu{}^\Omega]$. The translational velocity $\{\mathbf{u}^i\}=u^i\mathbf{i}^i+v^i\mathbf{j}^i+w^i\mathbf{k}^i$ and angular rate $\mathbf{\Omega}=p^i\mathbf{i}^i+q^i\mathbf{j}^i+r^i\mathbf{k}^i$ are given in a local ship-related coordinate system $O^ix^iy^iz^i$; see Fig. 2. The superscript $i=A, B$ indicates that a definition or description is common for both ships. The ship's position with respect to an inertial coordinate system $O^0x^0y^0z^0$ is defined by a position vector $\mathbf{R}^i$, and the orientation by Euler's angles $[\boldsymbol{\varphi}]=\left[\phi \quad \theta \quad \psi\right]^T$ between $O^ix^iy^iz^i$ and the horizontal body axes $O^i\xi^i\eta^i\zeta^i$. The horizontal body axes are subjected to translations only and thus their orientation with respect to the inertial coordinate system remains constant throughout the collision.

Here it is assumed that the effect of sloshing on the ship's mass center is negligible and that thus the origins O^i of these two local coordinate systems are both fixed to the initial mass center of gravity of the ship. This simplification is believed to have only a minor influence on the ship's response.

2.2. Extended equations of motion to consider sloshing

The linear sloshing model replaces the fluid mass m_T in a tank with a single rigidly fixed mass m_R and with a number of discrete mass-spring elements m_n; see Fig. 3. Each oscillating mass corresponds to one sloshing mode. The effect of a spring-mass element on the sloshing force decreases rapidly with an increase in the mode number. It was shown by Tabri et al. (2009a) that in collision applications it suffices if the total sloshing response is derived as a superposition of responses of three lowest

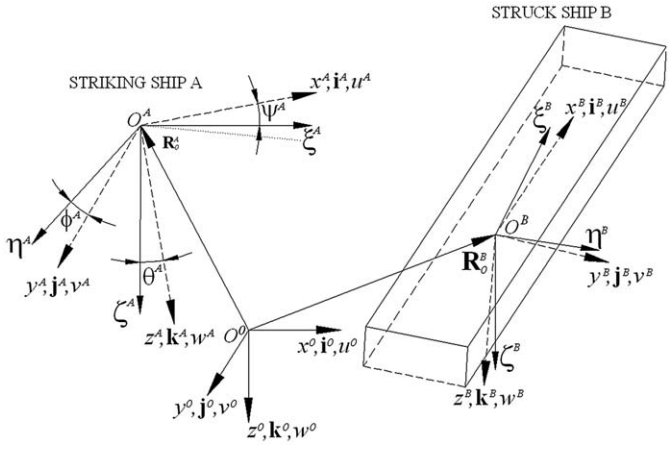

Fig. 2. Definition of coordinate systems and position vectors.

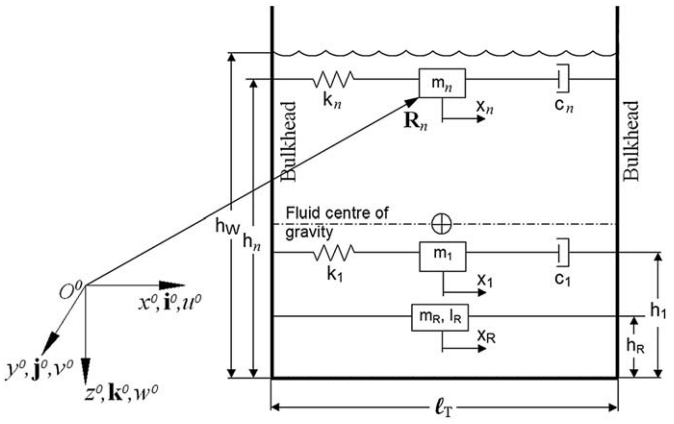

Fig. 3. Simplified discrete mechanical model for sloshing.

sloshing modes i.e. the number of oscillating masses in a single tank is three. The equation of translational motion for a single mass m_n connected to the tank walls by a spring of stiffness k_n and a damper with a damping coefficient c_n is

$$m_n\dot{u}_n + c_n(u_n - u) + k_n(x_n - x) = 0, \tag{3}$$

where in a local coordinate system $\dot{u}$, u, and x present the acceleration, velocity, and displacement of the tank, and $\dot{u}_n$, u_n, and x_n, correspondingly, those of the oscillating mass on the direction of a certain motion component. Here it is assumed that the angular motions do not influence the sloshing dynamics and vice versa. Thus, the sloshing interaction is considered only for sway and surge motions presented in the local coordinate system of the ship. On the basis of Graham and Rodriguez (1952) and Fig. 3, the formulations for the mass m_n and stiffness k_n of nth oscillating mass element are

$$m_n = m_T\left(\frac{8l_T}{\pi^2(2n-1)^3 h_W}\right)\tanh\left((2n-1)\pi\frac{h_W}{l_T}\right), \tag{4}$$

$$k_n = \omega_n^2 m_n = m_T\frac{8g}{\pi^2(2n-1)^2 h_W}\tanh\left((2n-1)\pi\frac{h_W}{l_T}\right)^2, \tag{5}$$

where h_W is the water height in the tank and l_T is the dimension of the tank in the sloshing direction. Correspondingly, the damping coefficient c_n is

$$c_n = \frac{\omega_n}{\pi}\delta, \tag{6}$$

where ω_n is the eigenfrequency of the nth oscillating mass and δ is the logarithmic decrement.

The total number of degrees of freedom, Q, associated with a ship is the sum of the rigid degrees of freedom, N_R, and the total number of oscillating masses J

$$Q = N_R + J \tag{7}$$

and $J=3I$ where I is the number of partially filled fluid tanks.

The equations of motion (Eq. (2)) are now extended to consider the sloshing interaction. Three new $Q\times Q$ matrices $[\mathrm{M}_n]$, $[\mathrm{C}_n]$, and $[\mathrm{K}_n]$, containing the m_n, c_n, and k_n terms and the vectors $\{\dot{\mathbf{u}}_n\}$, $\{\mathbf{u}_n\}$, and $\{\mathbf{x}_n\}$ containing the oscillating degrees of freedom in Eq. (3), are formed and combined with Eq. (2). Therefore, six $J\times J$ zero-matrices, denoted by [0], are formed and added to $[\mathbf{M}_\mu]$ and $[\mathbf{M}_\mu{}^{\Omega}]$ in order to account for the oscillating degrees of freedom. As a result this gives new equations of motion with Q degrees of freedom:

$$\left(\begin{bmatrix}[\mathbf{M}_\mu] & [0]\\ [0] & [0]\end{bmatrix} + [\mathbf{M}_n]\right)\begin{Bmatrix}\dot{\mathbf{u}}\\ \dot{\boldsymbol{\Omega}}\\ \dot{\mathbf{u}}_n\end{Bmatrix} + \left(\begin{bmatrix}[\mathbf{M}_\mu^{\Omega}] & [0]\\ [0] & [0]\end{bmatrix} + [\mathbf{C}_n]\right)\begin{Bmatrix}\mathbf{u}\\ \boldsymbol{\Omega}\\ \mathbf{u}_n\end{Bmatrix} + [\mathbf{K}_n]\begin{matrix}\{\mathbf{x}\}\\ [\boldsymbol{\varphi}]\\ \{\mathbf{x}_n\}\end{matrix} = \begin{Bmatrix}\mathbf{F}\\ \mathbf{G}\end{Bmatrix} - \mathbf{F}_\mu. \tag{8}$$

Eq. (8), containing in addition to rigid body motions also six oscillating degrees of freedom, is presented in the scalar form in Appendix B. Displacements are evaluated as the projections of the position vectors $\{\mathbf{R}\}$ and $\{\mathbf{R}_n\}$ to the local coordinate system $O^ix^iy^iz^i$ giving $\{\mathbf{x}\}=[\mathbf{T}]^T\{\mathbf{R}\}$ and $\{\mathbf{x}_n\}=[\mathbf{T}]^T\{\mathbf{R}_n\}$, where the orthogonal matrix of transformation (Clayton and Bishop, 1982) is, in component form

$$\begin{Bmatrix}x^0\\ y^0\\ z^0\end{Bmatrix} = [\mathbf{T}]\begin{Bmatrix}x^i\\ y^i\\ z^i\end{Bmatrix} = \begin{bmatrix}\cos\psi\cos\theta & \cos\psi\sin\theta\sin\phi - \sin\psi\cos\phi & \cos\psi\sin\theta\cos\phi + \sin\psi\sin\phi\\ \sin\psi\cos\theta & \sin\psi\sin\theta\sin\phi + \cos\psi\cos\phi & \sin\psi\sin\theta\cos\phi - \cos\psi\sin\phi\\ -\sin\theta & \cos\theta\sin\phi & \cos\theta\cos\phi\end{bmatrix} \times \begin{Bmatrix}x^i\\ y^i\\ z^i\end{Bmatrix}. \tag{9}$$

The time integration of the equations of motion is based on an explicit 5th-order Dormand–Prince integration scheme (Dormand and Prince, 1980), which is a member of the Runge-Kutta family of solvers. For time-efficient integration, the forces on the right-hand side of the Eq. (8) are kept constant during time step dt, while the motions on the left-hand side are updated in every sub-increment. Also the matrix $[\mathbf{M}_\mu{}^{\Omega}]$ is updated in every sub-increment as it contains the velocity terms. Definitions for the external forces $\mathbf{F}$ and $\mathbf{G}$ resulting from the surrounding water and the contact between the ships are provided in Tabri et al. (2009b).

The solution of Eq. (8) provides motions at the end of the integration increment. There, the new position of the ship with respect to the inertial frame is evaluated by time integrating over the velocities in the local coordinate system and transforming the translational displacement increments that are obtained to the inertial frame by the matrix $[\mathbf{T}]$. These increments are added to the position vector $\mathbf{R}^i$. The orientation is updated by adding the angular increments to the Euler's angles. Given the positions and the orientations, the penetration between the ships and thus, the contact force is calculated. Also the other external forces on the right-hand side are updated.

The equations of motion (Eq. (8)) are established for each ship. These equations are treated separately during the time integration increment and the mutual contact force is updated after each integration step in order to maintain the kinematic connection.

3. Model-scale collision experiments with sloshing interaction

An understanding of the sloshing physics was gained through a series of model-scale experiments carried out in the test basin of Helsinki University of Technology; see Fig. 4. An elaborate description of the ship models and their scaling is given in Tabri et al. (2007), where symmetric collision experiments without sloshing interaction are presented. Here, the additional modifications to the test setup and the measuring system necessary for the wet tests are described.

3.1. Test setup

The model tests were designed to be physically similar to the large-scale experiments (Wevers and Vredeveldt, 1999). The feasible scaling factor based on the Froude scaling law was $\lambda=35$ (Tabri et al., 2007).

To maintain the geometric similarity to the ships used in the large-scale experiments with a Y-core structure (Wevers and Vredeveldt, 1999), the models had the following main dimensions: length $L^A=L^B=2.29$ m, depth $D^A=D^B=0.12$ m, and breadth $B^A=0.234$ m for the striking ship and $B^B=0.271$ m for the struck ship. Two fluid tanks were installed on board the striking ship model, as shown in Figs. 4 and 5. There, the side height of the tanks was greater than that of the ship used in the large-scale test, so as to reduce the effect of roof impacts. In the model tests the length of each tank was about 1/4 of the total length of the model. The length of the tanks was exaggerated compared to the large-scale tests to get clearer picture of the phenomena. With these tank dimensions the striking ship resembled a large crude oil carrier or a novel river tanker where increased crashworthiness of the side structures allows larger and longer cargo tanks (van de Graaf et al., 2004).

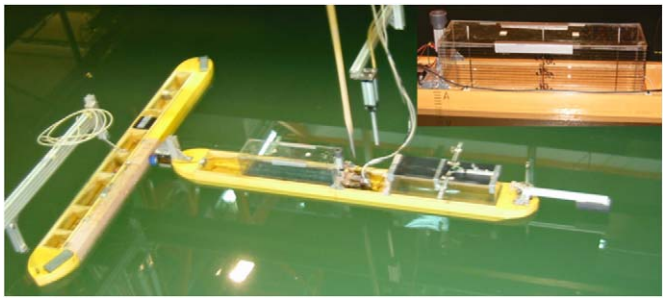

Fig. 4. Ship models with sloshing tanks on board the striking ship.

The striking ship model was equipped with an axi-symmetric rigid bulb, the dimensions of which are given in Fig. 6. In the struck ship model a block of polyurethane foam was installed at the location of the collision. The crushing strength of the foam was $\sigma=0.121$ MPa (Ranta and Tabri, 2007). The model-scale force–penetration curve was built up on the basis of this value and the shape of the contact surface. This force–penetration curve, presented in Fig. 7, corresponds well to that measured during the large-scale experiment with Y-core side structure (Tabri et al., 2009a, b) and scaled down with $\lambda=35$. Thus it can be stated that the dynamic similarity between the model-scale and large-scale experiments was roughly maintained.

The striking model was connected to the carriage of the test basin and it was accelerated smoothly to the desired collision velocity u_0^A to prevent sloshing before the collision. There was a connection between the carriage and the model situated close to the model's center of gravity in order to avoid initial pitch motion.

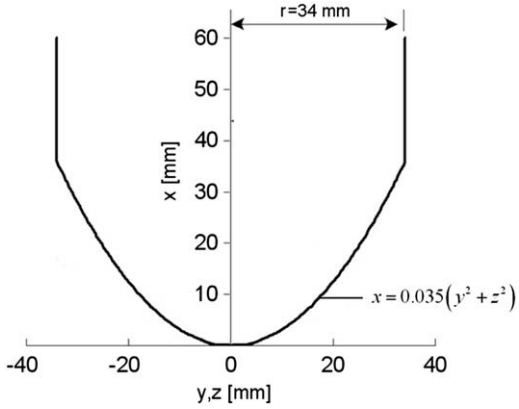

Fig. 6. Dimensions of the bulb used in the model-scale experiments.

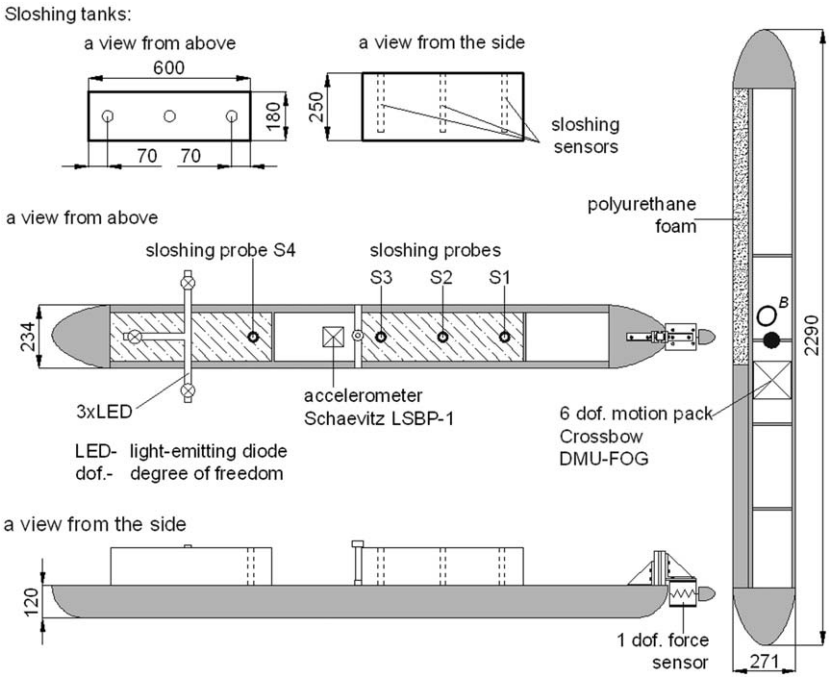

Fig. 5. Test setup with two sloshing tanks.

The struck model was fixed to the basin with line reels. Both models were released just before the contact.

All six motion components of the striking ship were recorded with respect to an inertial coordinate system with a Rodym DMM non-contact measuring system. This required as an input value the location of the center of gravity of the ship model. This value was considered constant during a collision. As discussed in Tabri et al. (2007), the post-processing in the Rodym system caused a time lag in the measured signals. In order to have precise synchronization with other measured signals, the longitudinal acceleration of the striking ship was also measured with a Schaevitz LSBP-1 accelerometer. All six motion components of the struck ship model were recorded by a Crossbow DMU-FOG motion pack installed on board the ship. This measuring system also provided time histories for the stabilized pitch and roll angles.

The free surface elevation in the sloshing tanks was measured with four resistive wave probes made of steel wire. Three probes were installed in the fore tank and one in the aft tank; see Fig. 5. The rigid bulb was connected to the striking ship via a force transducer (Tabri et al., 2007). The force was measured only in the longitudinal direction with respect to the striking ship model as the other components were expected to be negligible in symmetric collisions. All the signals were recorded with a sampling rate of 1.25 kHz, except those with the Rodym system, where the rate was 125 Hz.

Given the ship motions, the penetration time history was calculated based on the relative position between the ships, see Eq. (3) in Tabri et al. (2007). Combining the measured contact force and the penetration history results in a force–penetration curve, and the area under that curve gives the deformation energy E_D at the end of the collision process.

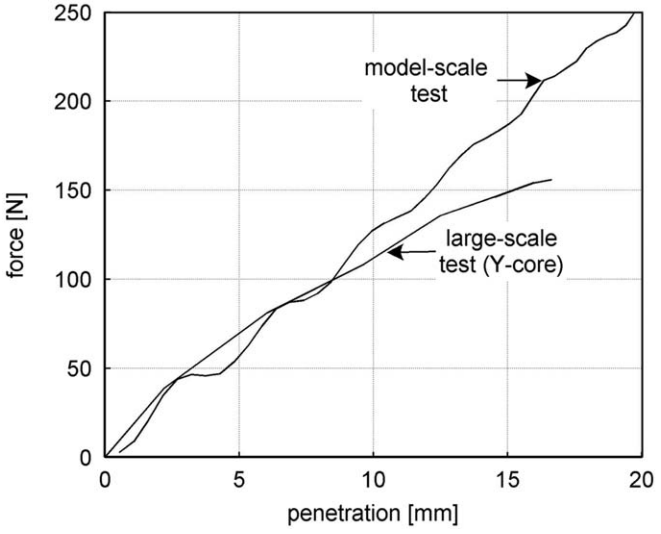

Fig. 7. Measured force–penetration curves in the large-scale and model-scale experiments. The large-scale measurement is scaled to model scale with $\lambda = 35$.

3.2. Test matrix

Four different loading conditions of the striking ship model were tested. These were based on the amount of water in the sloshing tanks, which varied from 21% to 47% of the total mass of the model. The tanks were filled in such a way that the model maintained an even keel condition, which resulted in slightly different amounts of water in the fore and aft tanks. Each loading condition was tested with three different collision velocities: 0.4, 0.7, and 1.0 m/s. Table C1 in Appendix C presents the test matrix for the different collision scenarios of the wet tests. The lightship mass of the striking ship without water was $m_{LS}^{A} = 22.1$ kg, except in the last three tests, where it was increased to 26.3 kg. The relative filling level, defined as a ratio between the water depth and the tank length h_W/ℓ_T, varied from 0.08 to 0.17. The mass of the struck ship was 30.5 kg throughout the tests.

To gain a deeper understanding of the influence of the sloshing interaction on the collision, most of the tests were repeated with a rigid mass replacing the water in tanks; see Table C2 in Appendix C for the full test matrix. These masses were positioned in such a way that the position of the ship's center of gravity remained unchanged.

The physical parameters of the ship models during the tests are presented in Table 1. The table presents the drafts, total masses, vertical height of the mass center of gravity *KG* measured from the base line of the model, longitudinal of gravity L_{COG} measured from the amidships, the radii of inertia k_{xx} and k_{yy} in relation to the x and y axes, and the calculated values for the ships' added masses. The radii of inertia with respect to the z-axis, k_{zz}, are assumed to be $k_{zz} = k_{yy}$. The radii are evaluated on the assumption of a still water level in the tanks. The non-dimensional added mass coefficients μ are based on

$$\mu_j = \lim_{\omega \to \infty} \frac{a_j(\omega)}{\rho \nabla}, \text{with } j = 2, 3, \tag{10}$$

for translational motions such as sway and heave, and correspondingly

$$\mu_j = \lim_{\omega \to \infty} \frac{a_j(\omega)}{\rho \nabla k_j^2}, \text{with } j = 4, 5, 6, \tag{11}$$

for rotational motions such as roll, pitch, and yaw. The water density is denoted by ρ and the volumetric displacement of the ship by ∇. The frequency-dependent added masses $a(\omega)$ are calculated with strip theory (Journée, 1992). The coefficients were first evaluated in a coordinate system with its origin located at the

Table 1
Physical parameters of the ship models during the test.

Model	Draft (cm)	Total mass (kg)	*KG* (cm)	L_{COG} (cm)	k_{xx} (cm)	k_{yy} (cm)	μ_2 (%)	μ_3 (%)	μ_4 (%)	μ_5 (%)	μ_6 (%)
Striking (wet)	5.5	28.1	8.1	−9.4	18	90	23	237	8	99	10
Striking (wet)	6.5	33.1	8.9	−9.0	18	94	27	203	7	77	11
Striking (dry)	6.5	33.5	8.7	−8.8	18	94	27	203	7	77	11
Striking (wet)	6.75	35.0	7.5	−6.6	18	82	28	195	6	99	15
Striking (dry)	6.75	35.1	6.8	−6.7	18	82	28	195	6	99	15
Striking (wet)	7.5	40.7	7.0	−7.0	18	78	31	179	6	99	18
Striking (dry)	7.5	41.1	6.8	−6.9	18	78	31	179	6	99	18
Struck	6	30.5	7.3	0	17	69	21	238	14	184	17

water plane and transferred to $O^i x^i y^i z^i$ considering the distance between the water plane and the center of gravity. The surge added mass μ_1 for both ship models is taken as being 5% of the total mass of the model.

4. Sloshing interaction in collision model tests

First, emphasis is laid on the effect of the sloshing interaction on the collision dynamics. The experimental results from a wet and a dry test are compared. Typical force time histories of a wet experiment (S1-V7) and of an equivalent dry test (N1-V7) are shown in Fig. 8. In the wet experiment the water in the tanks accounted for 37% of the total ship mass and the filling level h_W/ℓ_T in the fore tank was 0.08 and that in the aft tank 0.13. The collision speed in both experiments was 0.7 m/s.

A comparison of the contact force histories of these two tests indicates that the sloshing interaction lowered the magnitude of the first force peak. Thus, as a result of the sloshing, the striking ship seems to behave like a lighter ship. In the wet test in Fig. 8a, after the first peak the contact was lost for about 0.1 s and the ships came into contact again as the striking ship regained speed as a result of the sloshing wave hitting the front bulkhead of each tank; see Fig. 9. There, the time histories of free surface elevation are presented for the probes S1 and S4, which are close to the front bulkheads of both tanks.

Surge motions of the striking ship are presented in Fig. 10 and these are in obvious correlation with the fluid motions inside the tanks. The effect of sloshing was not that obvious on the other motion components.

Fig. 9 shows that the main period of sloshing is about 1.7 s, a value which is an order of magnitude longer than the duration of the first force peak, being about 0.1 s. This fact reveals that the interaction of the water is delayed with respect to other major phenomena, such as the contact between the ships. Fig. 9 indicates that the sloshing motion is damped out strongly during the first period, after which the sloshing amplitude continues to decrease slowly. The damping during the first contact force peak clearly affects the collision dynamics. The damping is physically determined by the logarithmic decrement, which can be calculated by comparing the amplitudes of the first two consecutive sloshing waves:

$$\delta = \ln\left(\frac{X_1}{X_2}\right), \tag{12}$$

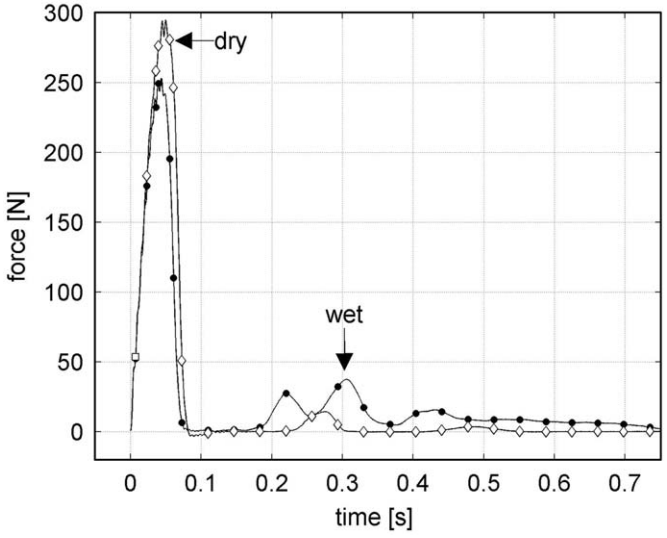

Fig. 8. Force history of a wet and an equivalent dry experiment (tests S1-V7 and N1-V7; see Tables C1 and C2).

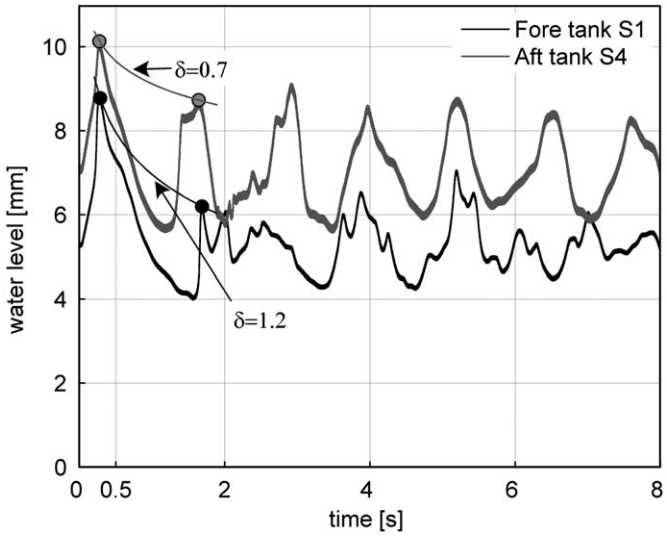

Fig. 9. Free surface elevation close to the front bulkhead of fore and aft tanks in test S1-V7.

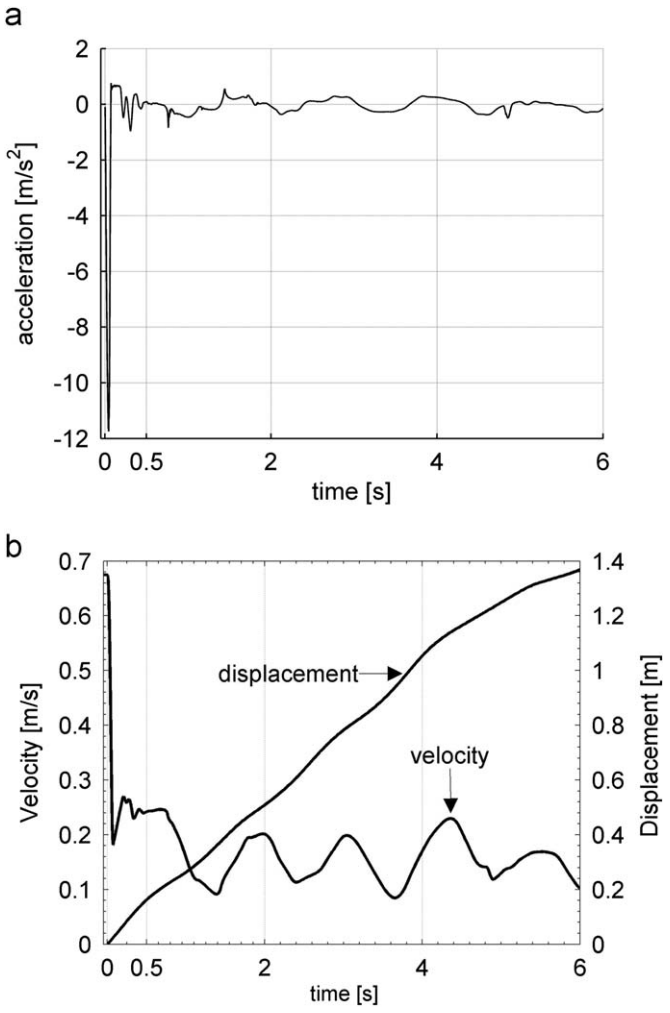

Fig. 10. Time histories of the acceleration (a), velocity and displacement (b) of the striking ship model in test S1-V7.

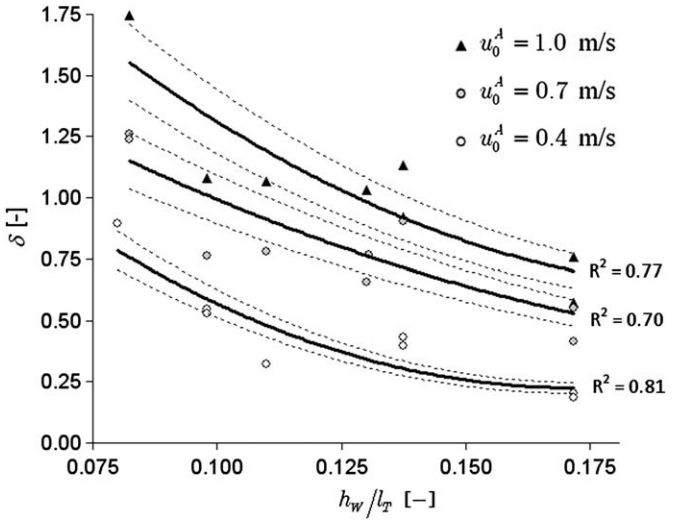

Fig. 11. Logarithmic damping decrement δ versus relative filling level and initial velocity as a parameter.

where X_1 indicates the amplitude of the first wave and correspondingly X_2 the second wave.

The decrement depends on the relative filling level h_W/ℓ_T and on the initial velocity of the striking ship model, as shown in Fig. 11. There, the calculated damping decrement δ is presented for each wet test and 2nd order polynomial regression curves are drawn for different initial velocities. The 10% error bounds presented with dashed lines and the R^2 values reveal relatively large deviation of the evaluated damping values. The sloshing is damped out faster in the case of a high initial velocity and a low relative filling level. It should be noted that this damping has only a minor effect on the maximum deformation energy in such a transient contact process. Its importance increases when dealing with the ship motions after the contact between the ships has been lost.

From the ship motions the relative displacement at contact, referred to as penetration, is calculated and its time history is presented in Fig. 12a. In the dry test the maximum penetration is deeper than that of the wet test. However, the second penetration peak is higher in the case of the wet test as a result of the sloshing interaction. The lower first penetration peak in the wet test gives

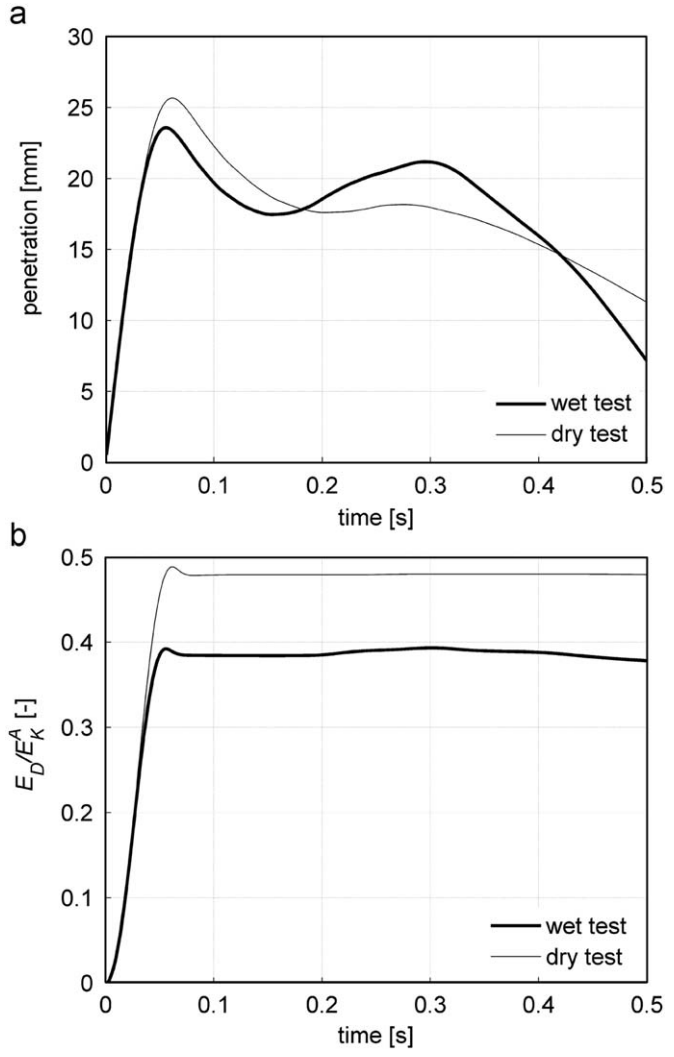

Fig. 12. Penetration (a) and relative deformation energy (b) in tests S1-V7 and N1-V7.

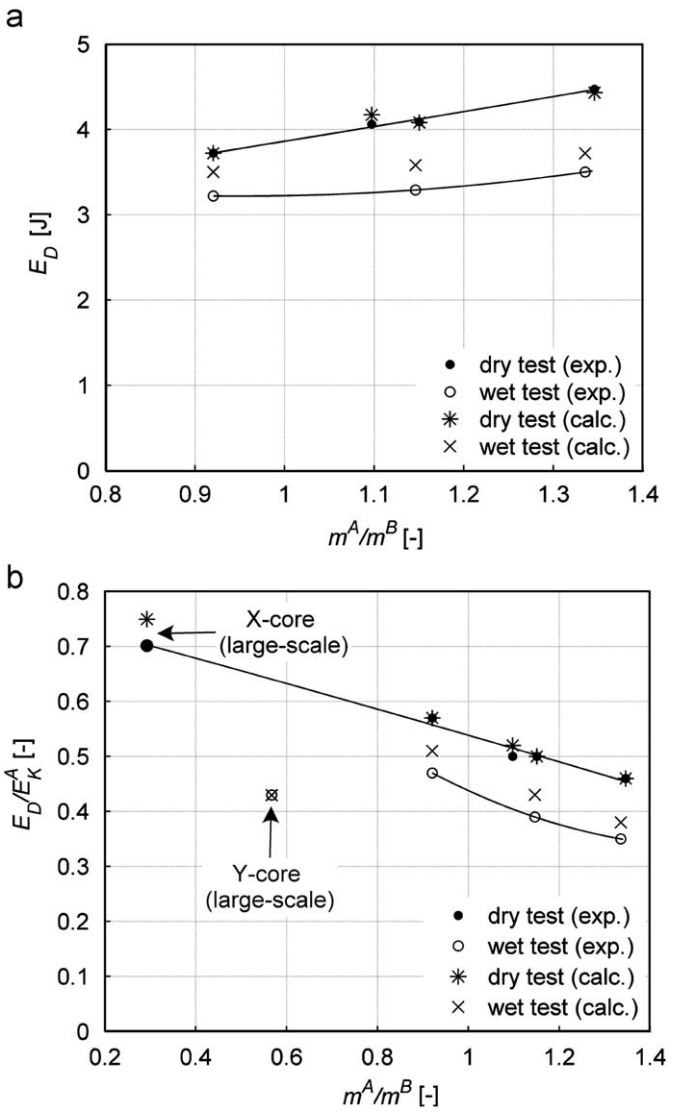

Fig. 13. Deformation energy (a) and relative deformation energy (b) as a function of mass ratio.

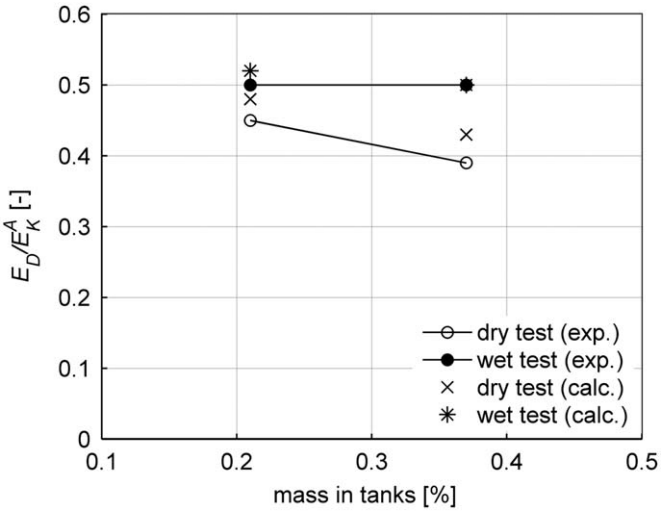

Fig. 14. Relative deformation energy as a function of sloshing mass (m^A/m^B= const.).

a smaller force value and thus the relative deformation energy $E_D/E_K^A|_{t=0}$ is only about 80% of that of the dry test; see Fig. 12b.

5. Influence of ship and water mass relation

The results of the numerical simulations are compared to those of the experiments. The numerical simulations are performed using the same parameter values as in the experiments and the damping coefficients c_n – see Eq. (6) – in the wet tests are evaluated using the decrement values taken from Fig. 11. The sensitivity of energy to the ship and water mass is presented in Figs. 13 and 14. There, the values are taken from the tests with a constant initial collision speed u_0^A=0.7 m/s.

The sensitivity study is based on two different approaches. First, the lightship mass is kept constant as $m_{LS}{}^A$=22.1 kg and the amount of water in the tanks varies; see Fig. 13. There, the structural deformation energy and the relative deformation energy versus the mass ratio of the ships are presented both for dry and wet tests. Fig. 13 demonstrates that the deformation energy in the wet tests is only about 80% of that of the dry tests. The correspondence between the calculated and the measured values is, on average, good. However, some overestimation in energy exists in the case of the wet tests, possibly as a result of the limitations of the sloshing model based on the linear potential flow theory. This discrepancy decreases as m^A and the water depth in the tanks increases.

This shortcoming of the sloshing model does not appear when we apply it to calculate the Y-core large-scale experiment (Tabri et al., 2009a, b); see Fig. 13b. In that large-scale collision experiment the relative filling levels in the tanks were higher, ranging from 0.1 to 0.4, and the calculations agree well with the measurements. The relative deformation energy of the Y-core experiment does not follow the trend of the wet model-scale tests as the sloshing took place in several tanks in both ships, yielding a greater energy reduction. In the other large-scale test with the X-core side structure (Tabri et al., 2009a, b), the situation was different as there was only a negligible amount of water in the tanks and thus the relative energy corresponds well to the trend of the dry model-scale tests. However, the numerical simulations slightly overestimate the deformation energy in the X-core test.

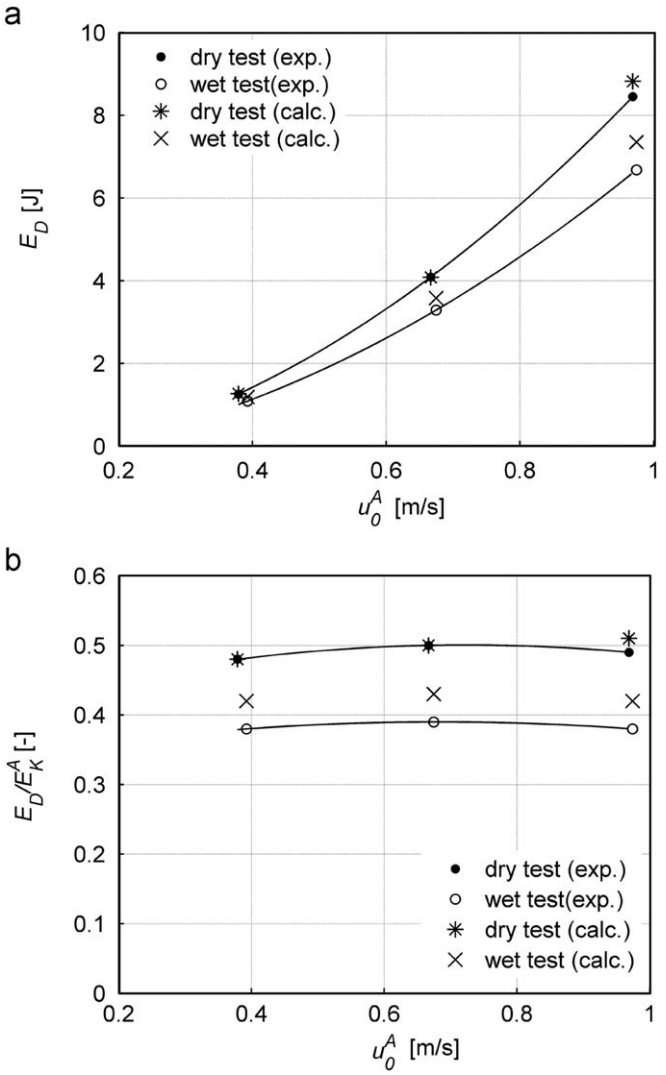

Fig. 15. Deformation energy (a) and relative deformation energy (b) versus initial velocity of the striking ship.

This previous presentation combines the effect of the ships' total masses and that of sloshing on the deformation energy. The pure effect of sloshing becomes more obvious when the tests are compared in which the ratio m^A/m^B and the initial velocity are constant, and the water or rigid mass in the tanks varies. This comparison is given in Fig. 14, where the results of the tests S1-V7, S4-V7, N1-V7, and N4-V7 are presented. As expected, in the dry tests the relative deformation energy remains unchanged as the mass ratio is constant. In the wet tests the relative deformation energy is reduced as the amount of the sloshing water increases.

6. Influence of initial collision velocity

The effect of the collision velocity on the deformation energy is studied by comparing the test results where all the parameters except the initial velocity are kept constant. The comparison is presented in Fig. 15.

Obviously, the velocity has a strong influence on the deformation energy in Fig. 15a. However, the relative deformation energy remains almost unchanged, as revealed by Fig. 15b. Thus, it can be concluded that the relative amount of kinetic energy "stored" in

the sloshing does not depend on the initial velocity of the striking ship. In addition, the deformation energy in the wet tests is still about 80% of that in the dry tests and the calculations continue to overestimate the deformation energy in the wet tests. This overestimation seems to be independent of the initial collision velocity.

7. Conclusions

The test setup developed for the wet tests proved to give reliable and repeatable results. The measuring equipment provided the opportunity to obtain valuable data for the understanding of the sloshing phenomenon and for the validation of the calculation models.

The results of the model-scale experiments emphasized the importance of sloshing interaction for collision dynamics. The influences of sloshing on the collision were due to the delayed transmission of momentum. Thus, the ship carrying liquid appears lighter and the resulting collision damage becomes less. The deformation energy in the wet test was only about 80% of that in the dry tests. Therefore, for the precise estimation of deformation energy in ship collision the sloshing effects have to be included. The relation between the masses of the participating ships had a significant effect on the deformation energy both in the dry and in the wet tests. The initial collision speed of the striking ship also had a strong influence on the deformation energy. However, this was not the case when the relative deformation energy was considered, as it remained almost unchanged as the velocity increased.

The calculation method that was developed overestimated the deformation energy by up to 10% in the case of the wet model-scale tests, but in the case of a large-scale wet test the predictions agreed well with the measurements. This overestimation is attributed to low relative filling levels, at which the linear sloshing model is at the boundary of its validity. In the large-scale experiment the filling levels were higher and the predictions agreed well. Thus it can be concluded that this discrete mechanical model of the sloshing gives satisfactory results for a certain limited range of water depths. However, more advanced CFD methods could enlarge the range of validity and also include the different geometries and structural arrangements inside the tanks.

More advanced calculations should provide the distribution of the sloshing pressure on the containing structure and thus, allow the strength of the tank walls to be analyzed. As the large amount of energy contained in sloshing is transmitted through the walls, the sloshing loads due to the collision could exceed the design sloshing loads of normal seagoing conditions.

Appendix A. Scalar form of equations of motion of a dry ship

The scalar form of equation of motion is based on the Newton's law and is given in the local coordinate system as (Clayton & Bishop, 1982)

$$\begin{cases} m(\dot{u}+qw-rv)=\mathbf{F}_x \\ m(\dot{v}+ru-pw)=\mathbf{F}_y \\ m(\dot{w}+pv-qu)=\mathbf{F}_z \\ I_x\dot{p}-I_{xy}\dot{q}-I_{xz}\dot{r}+(I_z r-I_{zx}p-I_{zy}q)q-(I_y q-I_{yz}r-I_{yx}p)r=\mathbf{M}_x \\ -I_{yx}\dot{p}+I_y\dot{q}-I_{yz}\dot{r}+(I_x p-I_{xy}q-I_{xz}r)r-(I_z r-I_{zx}p-I_{zy}q)p=\mathbf{M}_y \\ -I_{zx}\dot{p}-I_{zy}\dot{q}+I_z\dot{r}+(I_y q-I_{yz}r-I_{yx}p)p-(I_x p-I_{xy}q-I_{xz}r)q=\mathbf{M}_z \end{cases} \tag{A.1}$$

is presented in matrix form as

$$\begin{bmatrix} [\mathbf{M}] & 0 \\ 0 & [\mathbf{I}] \end{bmatrix} \begin{Bmatrix} \dot{\mathbf{u}} \\ \dot{\mathbf{\Omega}} \end{Bmatrix} + \begin{Bmatrix} [\mathbf{M}]\mathbf{\Omega}\times\mathbf{u} \\ \mathbf{\Omega}\times[\mathbf{I}]\mathbf{\Omega} \end{Bmatrix} = \begin{Bmatrix} \mathbf{F} \\ \mathbf{G} \end{Bmatrix}. \tag{A.2}$$

For numerical integration, Eq. (A.2) is rearranged to obtain a more convenient form by introducing matrices $[\mathbf{M}_\mu]$ and $[\mathbf{M}_\mu{}^{\Omega}]$, which contain the added mass and the non-linear acceleration terms:

$$[\mathbf{M}_\mu]\begin{Bmatrix} \dot{\mathbf{u}} \\ \dot{\mathbf{\Omega}} \end{Bmatrix} + [\mathbf{M}_\mu^{\Omega}]\begin{Bmatrix} \mathbf{u} \\ \mathbf{\Omega} \end{Bmatrix} = \begin{Bmatrix} \mathbf{F} \\ \mathbf{G} \end{Bmatrix} - \mathbf{F}_\mu, \tag{A.3}$$

As the acceleration component of the radiation force $\mathbf{F}_\mu$ is already included through the matrices in the left-hand side, it should be subtracted from the right-hand side. The matrices have the following component form:

$$[\mathbf{M}_\mu] = \begin{bmatrix} m+a_1 & 0 & 0 & 0 & a_{15} & 0 \\ 0 & m+a_2 & 0 & a_{24} & 0 & a_{26} \\ 0 & 0 & m+a_3 & 0 & a_{35} & 0 \\ 0 & a_{42} & 0 & I_x+a_{44} & 0 & -I_{xz} \\ a_{51} & 0 & a_{53} & 0 & I_y+a_{55} & 0 \\ 0 & a_{62} & 0 & -I_{xz} & 0 & I_x+a_{66} \end{bmatrix}, \tag{A.4}$$

$$[\mathbf{M}_\mu^{\Omega}] = \begin{bmatrix} 0 & -(m+a_1)r & (m+a_1)q & 0 & 0 & 0 \\ (m+a_2)r & 0 & -(m+a_2)p & 0 & 0 & 0 \\ -(m+a_3)q & (m+a_3)p & 0 & 0 & 0 & 0 \\ 0 & 0 & 0 & 0 & I_{45} & -I_{46} \\ 0 & 0 & 0 & -I_{45} & 0 & I_{56} \\ 0 & 0 & 0 & I_{46} & -I_{56} & 0 \end{bmatrix}, \tag{A.5}$$

with

$$I_{45}=(I_z+a_{66})r-(I_{zx}+a_{64})p-I_{zy}q,$$
$$I_{46}=(I_y+a_{55})q-I_{yz}r-I_{yx}p,$$
$$I_{56}=(I_x+a_{44})p-I_{xy}q-(I_{xz}+a_{46})r.$$

and the following concept is used to abbreviate the definitions for moments of inertia:

$$I_x=\rho(y^2+z^2)dV,$$

$$I_{xy}=\rho xydV,$$

where V is the volume of the body. For the sake of clarity, the subscripts 1, 2, 3, 4, 5, 6 are used to denote the added masses for surge, sway, heave, roll, pitch, and yaw, respectively.

Appendix B. Scalar form of extended equations of motion of a wet ship

The equations of motion of a wet ship are defined as

$$\left(\begin{bmatrix} [\mathbf{M}_\mu] & [0] \\ [0] & [0] \end{bmatrix} + [\mathbf{M}_n]\right)\begin{Bmatrix} \dot{\mathbf{u}} \\ \dot{\mathbf{\Omega}} \\ \dot{\mathbf{u}}_n \end{Bmatrix} + \left(\begin{bmatrix} [\mathbf{M}_\mu^{\Omega}] & [0] \\ [0] & [0] \end{bmatrix} + [\mathbf{C}_n]\right)\begin{Bmatrix} \mathbf{u} \\ \mathbf{\Omega} \\ \mathbf{u}_n \end{Bmatrix} + [\mathbf{K}_n]\begin{Bmatrix} \{\mathbf{x}\} \\ [\varphi] \\ \{\mathbf{x}_n\} \end{Bmatrix} = \begin{Bmatrix} \mathbf{F} \\ \mathbf{G} \end{Bmatrix} - \mathbf{F}_\mu, \tag{13}$$

The mass matrix $[\mathbf{M}_\mu]$ includes the total ship mass and inertia without distinguishing between the lightship mass m_{LS} and the oscillating masses m_n. The sloshing mass matrix $[\mathbf{M}_n]$ removes the

oscillating masses from the total mass matrix and assigns them to appropriate sloshing degrees of freedom. The sloshing mass matrix is defined as

$$[\mathbf{M}_n]=\begin{bmatrix} -\sum_{n=1}^{3} m_{n,x} & 0 & \cdots & 0 & 0 & 0 & 0 & 0 & 0 \\ 0 & -\sum_{n=1}^{3} m_{n,y} & \cdots & 0 & 0 & 0 & 0 & 0 & 0 \\ \vdots & \vdots & \ddots & \vdots & \vdots & \vdots & \vdots & \vdots & \vdots \\ 0 & 0 & \cdots & m_{1,x} & 0 & 0 & 0 & 0 & 0 \\ 0 & 0 & \cdots & 0 & m_{2,x} & 0 & 0 & 0 & 0 \\ 0 & 0 & \cdots & 0 & 0 & m_{3,x} & 0 & 0 & 0 \\ 0 & 0 & \cdots & 0 & 0 & 0 & m_{1,y} & 0 & 0 \\ 0 & 0 & \cdots & 0 & 0 & 0 & 0 & m_{2,y} & 0 \\ 0 & 0 & \cdots & 0 & 0 & 0 & 0 & 0 & m_{3,y} \end{bmatrix} \tag{B.1}$$

The subscript indices x and y denote surge and sway, respectively. The degrees of freedom associated with heave and angular motions are truncated for the sake of brevity as it is assumed that they are not affected by the sloshing.

According to Eq. (3) each mass element appears twice for a corresponding degree of freedom in $[\mathbf{C}_n]$ and $[\mathbf{K}_n]$, accounting first for the rigid body motion and second for the oscillatory motion. Considering this, the damping matrix is defined as

$$[\mathbf{C}_n]=\begin{bmatrix} \sum_{n=1}^{3} c_{n,x} & 0 & \cdots & -c_{1,x} & -c_{2,x} & -c_{3,x} & 0 & 0 & 0 \\ 0 & \sum_{n=1}^{3} c_{n,y} & \cdots & 0 & 0 & 0 & -c_{1,y} & -c_{2,y} & -c_{3,y} \\ \vdots & \vdots & \ddots & \vdots & \vdots & \vdots & \vdots & \vdots & \vdots \\ -c_{1,x} & 0 & \cdots & c_{1,x} & 0 & 0 & 0 & 0 & 0 \\ -c_{2,x} & 0 & \cdots & 0 & c_{2,x} & 0 & 0 & 0 & 0 \\ -c_{3,x} & 0 & \cdots & 0 & 0 & c_{3,x} & 0 & 0 & 0 \\ 0 & -c_{1,y} & \cdots & 0 & 0 & 0 & c_{1,y} & 0 & 0 \\ 0 & -c_{2,y} & \cdots & 0 & 0 & 0 & 0 & c_{2,y} & 0 \\ 0 & -c_{3,y} & \cdots & 0 & 0 & 0 & 0 & 0 & c_{3,y} \end{bmatrix}, \tag{B.2}$$

and the stiffness matrix as

$$[\mathbf{K}_n]=\begin{bmatrix} \sum_{n=1}^{3} k_{n,x} & 0 & \cdots & -k_{1,x} & -k_{2,x} & -k_{3,x} & 0 & 0 & 0 \\ 0 & \sum_{n=1}^{3} k_{n,y} & \cdots & 0 & 0 & 0 & -k_{1,y} & -k_{2,y} & -k_{3,y} \\ \vdots & \vdots & \ddots & \vdots & \vdots & \vdots & \vdots & \vdots & \vdots \\ -k_{1,x} & 0 & \cdots & k_{1,x} & 0 & 0 & 0 & 0 & 0 \\ -k_{2,x} & 0 & \cdots & 0 & k_{2,x} & 0 & 0 & 0 & 0 \\ -k_{3,x} & 0 & \cdots & 0 & 0 & k_{3,x} & 0 & 0 & 0 \\ 0 & -k_{1,y} & \cdots & 0 & 0 & 0 & k_{1,y} & 0 & 0 \\ 0 & -k_{2,y} & \cdots & 0 & 0 & 0 & 0 & k_{2,y} & 0 \\ 0 & -k_{3,y} & \cdots & 0 & 0 & 0 & 0 & 0 & k_{3,y} \end{bmatrix}. \tag{B.3}$$

Table C1
Collision experiments with sloshing.

Name	u_0^A (m/s)	$m_{LS}{}^A$ (kg)	Water mass		h_W/ℓ_T		Amount of water (%)	m^A/m^{B*} (–)	E_D	
			fore (kg)	aft (kg)	fore (–)	aft (–)			exp. (J)	calc. (J)
S1-V4	0.4	22.1	5.0	8.0	0.08	0.13	37	1.15	1.1	1.2
S1-V7	0.7	22.1	5.0	8.0	0.08	0.13	37	1.15	3.3	3.6
S1-V10	1.0	22.1	5.0	8.0	0.08	0.13	37	1.15	6.7	7.3
S2-V4	0.4	22.1	8.4	10.5	0.14	0.17	47	1.34	1.3	1.2
S2-V7	0.7	22.1	8.4	10.5	0.14	0.17	47	1.34	3.5	3.7
S2-V10	1.0	22.1	8.4	10.5	0.14	0.17	47	1.34	6.5	7.1
S3-V4	0.4	22.1	0.0	6.0	0.00	0.10	21	0.92	1.1	1.1
S3-V7	0.7	22.1	0.0	6.0	0.00	0.10	21	0.92	3.2	3.5
S3-V10	1.0	22.1	0.0	6.0	0.00	0.10	21	0.92	6.4	6.9
S4-V4	0.4	26.3	6.8	0.0	0.11	0.00	21	1.08	1.2	1.2
S4-V7	0.7	26.3	6.8	0.0	0.11	0.00	21	1.08	3.6	3.8
S4-V10	1.0	26.3	6.8	0.0	0.11	0.00	21	1.08	7.3	7.7

$u_0{}^A$ is the collision velocity.
$m_{LS}{}^A$ is the lightship mass of the striking ship.

* is the m^B=30.5 kg throughout the experiments.

Table C2
Collision experiments with fixed masses.

Name	u_0^A (m/s)	$m_{LS}{}^A$ (kg)	Water mass		h_W/ℓ_T		Amount of water (%)	m^A/m^{B*} (–)	E_D	
			fore (kg)	aft (kg)	fore (–)	aft (–)			exp. (J)	calc. (J)
N1-V4	0.4	22.1	5.0	8.0	–	–	–	1.15	1.3	1.3
N1-V7	0.7	22.1	5.0	8.0	–	–	–	1.15	4.1	4.1
N1-V10	1	22.1	5.0	8.0	–	–	–	1.15	8.6	8.8
N2-V4	0.4	22.1	8.5	10.5	–	–	–	1.35	1.5	1.6
N2-V7	0.7	22.1	8.5	10.5	–	–	–	1.35	4.5	4.4
N2-V10	1	22.1	8.5	10.5	–	–	–	1.35	8.6	8.9
N4-V4	0.4	26.5	7.0	0.0	–	–	–	1.10	1.3	1.4
N4-V7	0.7	26.5	7.0	0.0	–	–	–	1.10	4.1	4.2
N4-V10	1	26.5	7.0	0.0	–	–	–	1.10	8.2	8.7

$u_0{}^A$ is the collision velocity.
$m_{LS}{}^A$ is the lightship mass of the striking ship.

* is the m^B=30.5 kg throughout the experiments.

Appendix C. Model-scale experiments

See Appendix Tables C1 and C2.

References

Brown, A.J., 2002. Collision scenarios and probabilistic collision damage. Marine Structures 15 (4–5), 335–364.

Chen, Y.G., Djidjeli, K., Price, W.G., 2008. Numerical simulation of liquid sloshing phenomena in partially filled containers, Computers & Fluids, doi:10.1016/j.compfluid.2008.09.003.

Clayton, B.R., Bishop, R.E.D., 1982. Mechanics of Marine Vehicles. E.F.N. Spon Ltd., London.

Dormand, J.R., Prince, P.J., 1980. A family of embedded Runge-Kutta formulae. Journal of Computational and Applied Mathematics 6 (1), 19–26.

Graham, E.W., Rodriguez, A.M., 1952. The characteristics of fuel motion which affect airplane dynamics. Transactions of ASME, Series E, Journal of Applied Mechanics 19 (3), 381–388.

Journée, J.M.J., 1992. Strip theory algorithms. Delft University of Technology, Report MEMT 24.

Minorsky, V.U., 1959. An analysis of ship collision with reference to protection of nuclear power plants. Journal of Ship Research 3, 1–4.

Petersen, M.J., 1982. Dynamics of ship collisions. Ocean Engineering 9 (4), 295–329.

Ranta, J., Tabri, K., 2007. Study on the Properties of Polyurethane Foam for Model-Scale Ship Collision Experiments. Helsinki University of Technology, Report M-297.

Tabri, K., Broekhuijsen, J., Matusiak, J., Varsta, P., 2009a. Analytical modelling of ship collision based on full-scale experiments. Marine Structures 22 (1), 42–61.

Tabri, K., Määttänen, J., Ranta, J., 2007. Model-scale experiments of symmetric ship collisions. Journal Marine Science and Technology 13 (1), 71–84.

Tabri, K., Varsta, P., Matusiak, J., 2009b. Numerical and experimental motion simulations of non-symmetric ship collisions. Journal of Marine Science and Technology, submitted for publication.

van de Graaf, B., Broekhuijsen, J., Vredeveldt, A., van de Ven, A., 2004. Construction aspects for the schelde Y-shape crashworthy hull structure. In: Proceedings of 3rd International Conference on Collision and Grounding of Ships ICCSG 2004, Tokyo, Japan.

Wevers, L.J., Vredeveldt, A.W., 1999. Full Scale Ship Collision Experiments 1998, TNO report 98-CMC-R1725, Delft, The Netherlands.

Wolf, M., 2003. Full scale collision experiment, X-type Sandwich side hull, EU Sandwich project report Deliverable TRD448.

Zhang, A., Suzuki, K., 2007. A comparative study of numerical simulations for fluid structure interaction of liquid-filled tank during ship collision. Ocean Engineering 34 (5–6), 645–652.